Society For Biomaterials

Removable partial denture alloys processed by laser-sintering technique

Omar Alageel,[1,2] Mohamed-Nur Abdallah ,[1] Ammar Alsheghri,[3] Jun Song,[3] Eric Caron,[4] Faleh Tamimi[1]

[1]Faculty of Dentistry, McGill University, Montreal, Quebec, Canada
[2]College of Applied Medical Sciences, King Saud University, Riyadh, Saudi Arabia
[3]Department of Mining and Materials Engineering, McGill University, Montreal, Quebec, Canada
[4]3DRPD Inc., Montreal, Quebec, Canada

Received 9 November 2016; revised 3 May 2017; accepted 12 May 2017
Published online 31 May 2017 in Wiley Online Library (wileyonlinelibrary.com). DOI: 10.1002/jbm.b.33929

Abstract: Removable partial dentures (RPDs) are traditionally made using a casting technique. New additive manufacturing processes based on laser sintering has been developed for quick fabrication of RPDs metal frameworks at low cost. The objective of this study was to characterize the mechanical, physical, and biocompatibility properties of RPD cobalt–chromium (Co–Cr) alloys produced by two laser-sintering systems and compare them to those prepared using traditional casting methods. The laser-sintered Co–Cr alloys were processed by the selective laser-sintering method (SLS) and the direct metal laser-sintering (DMLS) method using the Phenix system (L-1) and EOS system (L-2), respectively. L-1 and L-2 techniques were 8 and 3.5 times more precise than the casting (CC) technique ($p < 0.05$). Co–Cr alloys processed by L-1 and L-2 showed higher ($p < 0.05$) hardness (14–19%), yield strength (10–13%), and fatigue resistance (71–72%) compared to CC alloys. This was probably due to their smaller grain size and higher microstructural homogeneity. All Co–Cr alloys exhibited low porosity (2.1–3.3%); however, pore distribution was more homogenous in L-1 and L-2 alloys when compared to CC alloys. Both laser-sintered and cast alloys were biocompatible. In conclusion, laser-sintered alloys are more precise and present better mechanical and fatigue properties than cast alloys for RPDs. © 2017 Wiley Periodicals, Inc. J Biomed Mater Res Part B: Appl Biomater, 106B: 1174–1185, 2018.

Key Words: laser-sintering, cobalt–chromium (Co–Cr), removable partial dentures, fatigue resistance, biocompatibility

How to cite this article: Alageel O, Abdallah MN, Alsheghri A, Song J, Caron E, Tamimi F. 2018. Removable partial denture alloys processed by laser-sintering technique. J Biomed Mater Res Part B 2018:106B:1174–1185.

INTRODUCTION

Removable partial dentures (RPDs) are simple and cost-effective prostheses that can restore missing teeth in partially edentulous patients, and thus improving their quality of life.[1,2] This type of treatment has an important impact on the life of millions of patients in the world; indeed, over 13% of the adult population in North America and Europe wear RPDs.[1,3] RPD frameworks are commonly made of cobalt–chromium (Co–Cr) alloys because of their suitable cost and mechanical properties, and their excellent corrosion resistance and biocompatibility.[4]

RPD frameworks are traditionally fabricated using the casting (lost-wax) technique that has been used in dentistry for more than a century.[5,6] The casting technique is a very laborious manual process that involves making a wax replica of the object, making a mold of the object, and then cast the melted metal into the mold. Owing to its complexity, this technique is strongly influenced by the skill of the dental technician.[5,7] Moreover, producing RPDs by casting technique not only is time consuming and costly but may also generates low precision and ill-fitting frameworks.[7,8]

Different methods were introduced in the last few decades for fabricating RPD frameworks without using casting techniques.[6,9,10] A new additive manufacturing (AM) process based on laser-sintering has been developed for processing 3-D metal objects. The laser-sintering technique combines computer-aided design (CAD) of any products and their subsequent fabrication using a high-power laser that fuses metal powder in a layer-by-layer pattern.[5,6,10–12] The laser-sintering technique enables the fabrication of complex 3-D objects quickly with high precision (20 μm) and at low cost.[10–15]

Laser-sintering technology can be described using different terminologies, such as selective laser melting (SLM), selective laser-sintering (SLS), or direct metal laser-sintering (DMLS).[6,9,12,13] SLM involves full melting of the metal

Correspondence to: F. Tamimi, BDS, MSc, MClinDent, PhD; e-mail: faleh.tamimimarino@mcgill.ca
Contract grant sponsors: King Saud University (Riyadh, Saudi Arabia), 3DRPD Inc., and Natural Sciences and Engineering Research Council (NSERC) Collaborative Research Development
Contract grant sponsor: Fonds de recherche du Québec – Nature et technologies (FRQNT)
Contract grant sponsor: Fondation de l'Ordre des dentists du Quebec (FODQ)

TABLE I. The Manufactures Chemical Composition of the Cast (CC) and Laser-Sintered (L-1 and L-2) Co–Cr Alloys

Mass %	Cobalt (Co)	Chromium (Cr)	Molybdenum (Mo)	Silicon (Si)	Manganese (Mn)	Iron (Fe)	Tungsten (W)
CC	64	28.5	5.3	<1	<1	<1	–
L-1	63	29	5.5	<1	<1	<1	–
L-2	64	25	5.1	1	<1	<1	5

powder; while, both SLS and DMLS involve partial melting of some the metal powder, particularly melting at the surface of the particle.[12–14] The main difference between SLS and DMLS is that SLS powder can be metal or other materials (e.g., ceramic or polymer), and the powder only partially melts during the process,[12–16] whereas DMLS uses a mixture of metal powders with different melting temperatures (high or low).[12–14,16–18] During the DMLS process, the powder with the low melting temperature fully melts while the powder with high melting temperature partially melts.[12,13,16] In this study, we used two systems that are commercially available for dental applications; the Phenix system (Phenix, Riom, France) that is based on the SLS method, and the EOS system (EOS, Krailling, Germany) that is based on the DMLS approach.[12–16]

Fabricating RPDs using the laser-sintering technique, instead of casting technique, could increase the quality of RPDs and render the treatment less expensive and more accessible to a larger portion of the population.[6] However, the fabrication of Co–Cr RPDs by laser-sintering technology can affect the mechanical, physical, and biocompatibility properties of the alloys and subsequently affect the clinical performance of RPDs.[8,19,20] The properties of laser-sintered alloys can be influenced by differences in the fabrication process, such as laser beam power, scanning speed, metals powder size, and layer thickness.[8,19–21]

The mechanical property, such as elastic modulus and bending yield strength, is crucial for RPD because it prevents clasps, the retentive element of RPD, from catastrophic failure during the repetitive cycles of insertion and removal of the dentures from the mouth.[22,23] However, there is no data currently available on fatigue resistance of laser-sintered RPD alloys. Previous studies evaluated the physical properties including microstructure, corrosion resistance, and solubility of laser-sintered Co–Cr alloys for other applications.[8,20,21,24,25] These studies showed that laser-sintered alloys had better physical properties than cast Co–Cr alloys. In addition, the biocompatibility of cast Co–Cr alloy has been previously investigated.[26] Although the Co–Cr alloys produced by DMLS (EOS) system is certified by the ISO 9693 and ISO 10993, the biocompatibility of RPD Co–Cr produced by SLS (Phenix) system remains unknown.[8,27] Therefore, the objective of this study was to characterize and understand the mechanical properties, physical properties, and biocompatibility of RPD Co–Cr alloys produced by two different laser-sintering systems and to compare them to those made by the traditional casting method.

MATERIALS AND METHODS

Sample preparation

All experiments were performed using dental Co–Cr alloys. The chemical composition of the Co–Cr ingot and powder as provided by the manufacturers is listed in Table I. Co–Cr samples were fabricated by conventional casting (CC group), selective laser-sintering (SLS) method (L-1 group), and direct metal laser-sintering (DMLS) method (L-2 group) at the prototyping center (3DRPD Inc., Montreal, QC, Canada). Samples were prepared in different geometries according to the property under investigation. All samples were designed using a CAD system. The cast alloys (CC group) were fabricated following similar steps used for fabricating traditional RPD. The wax-ups of the CC samples were printed in a plastic form using a 3-D printer (UtraHD, EnvisionTEC, Dearborn, MI), invested in metal casting rings, and cast using an automatic vacuum-pressure casting machine with induction heating (Nautilus CC, BEGO, Bremen, Germany) using an ingot form of Co–Cr alloy (NobilStar Ultra; Nobilium, Albany, NY).

Two laser-sintering systems equipped with their specified Co–Cr powders were used to fabricate the L-1 and L-2 samples. L-1 samples were processed by the selective laser-sintering (SLS) technology using the PXM system (Phenix Systems, Riom, France) with 300 W of Fibre laser power and wavelength of 1070 nm and equipped with a roller to compact the powder. The particle size of the Co-Cr powder in the L-1 group (ST2724G-A, Sint-Tech; Clermont-Ferrand, France) as observed by the scanning electron microscope (SEM) was 6–22 μm. On the other hand, L-2 samples were processed using the EOSINT M270 system (EOS, Krailling, Germany), which is based on the direct metal laser-sintering (DMLS) approach, with 200 W of Fibre laser power and 1064 nm wavelength. The average particle size of the Co–Cr powder (CobaltChrome SP2, EOS; Krailling, Germany) in the L-2 group was 20 μm.[28] For both L-1 and L-2 samples, the layer thickness, the laser scan speed, and building direction were 30 μm, 5–7 m/s, and 90° respectively. Postprocessing heat treatments were applied to the L-1 and L-2 samples according to the manufacturers' instructions (L-1: 800°C for 30 min; L-2: 450°C for 45 min, 750°C for 60 min and then cooled down). Alloy samples for microhardness and crystallography were manually polished to produce a mirror-like surface using a six-step polishing process.[29]

Precision error calculation

The dimensions of the samples used for toughness analysis were measured with an electronic caliper (Fower, Newton, MA) to calculate the precision error of CC, L-1, and L-2 techniques. For each sample, the dimension of each sample was measured for all the 3 side surfaces (length, width, and thickness). Then, the dimensional changes between the processed and the CAD designed samples were calculated.

Mechanical characterization

Three-point bending tests, which are mimicking the fracture of RPDs clasps, were done at room temperature using a universal testing machine (Instron, 5569, Grove City, PA) to characterize the mechanical properties of CC, L-1, and L-2 alloys. Each sample ($n = 9$) was placed on two supporting pins 18 mm apart of each other. Loading was applied through an actuator by moving the loading pin at a constant speed of 1 mm/min on the middle of the specimen until failure. The testing machine then provided a force/deflection curve for each sample through the Bluehill v.2 software (Instron, Grove City, PA). The elastic modulus (E), bending yield strength (σ_y), flexural strength (σ_F), and fracture toughness (K_{1C}) values were calculated using Eqs. (1–5).[30–32]

$$E = \frac{F_{max} L^3}{4\delta b d^3} \tag{1}$$

$$\sigma_y = \frac{3F_y L}{2bd^2} \tag{2}$$

$$\sigma_F = \frac{3F_{max} L}{2bd^2} \tag{3}$$

$$K_{IC} = \frac{3F_{max} L}{2bd^2 \ Y\left(\frac{a}{b}\right)\sqrt{a}} \tag{4}$$

where

$$Y\left(\frac{a}{b}\right) = 1.93 - 3.07\left(\frac{a}{b}\right) + 14.5\left(\frac{a}{b}\right)^2 + 25.1\left(\frac{a}{b}\right)^3 + 25.8\left(\frac{a}{b}\right)^4 \tag{5}$$

where F_y is the yield force, F_{max} is the maximum force applied, L is the distance between the supports, δ is the deflection of the tested specimen, b is the width of the tested specimen, d is the height of the tested specimen, and a is the notch depth.

To determine the fatigue resistance of the CC, L-1, and L-2 alloys, 6 rectangular specimens from each group were exposed to a cyclic of three-point bending loading and unloading up to 6000 cycles. At each cycle, the load was applied at a constant speed of 15 mm/min until reaching a constant deflection of 0.2 and 0.1 mm, as these deflections are similar to the depth of undercuts on the abutment tooth surface where the RPD clasps engage with.[2] Then, the loading was repeated at a frequency of 5 Hz, and the force change (N) was recorded at each cycle. Finally, the postfatigue force was compared to their initial force to evaluate the fatigue resistance.

A Vickers microhardness indenter (Clark CM100 AT, HT-CM-95605, Shawnee Mission, KS) was employed on the polished surfaces of the Co–Cr samples. Tooth enamel sections fixed in resin blocks were also analyzed for comparison.[33,34] Nine measurements were obtained per specimen ($n = 3$) under indentation load of 500 g for 10 s of dwell time. Computer software (Vision PE 3.5, Clemex Technologies Inc., Shawnee Mission, KS) was used to measure the microhardness value at the site of indentation from images captured by a built-in camera.

Physical characterization

Density and porosity of the CC, L-1, and L-2 alloys were analyzed using five samples per group. The bulk density, which includes the volume of pore spaces in the alloys, was calculated by dividing the sample's weight by its volume. While, the real volume and real density (grain density), which do not include the pore spaces in the alloys, were measured using helium pycnometry (Accupyc 1330; Micromeretics; Bedfordshire, UK). Helium pycnometry measures the gas pressure in a calibrated chamber before and after insertion of the specimen into the chamber. Porosity percentage was calculated using the equation below [Eq. (6)].

$$\text{Porosity percentage} = \frac{(\text{bulk volume} - \text{real volume})}{\text{bulk volume}} \times 100 \tag{6}$$

To further analyze the porosity of the CC, L-1, and L-2 alloys, the specimens were scanned using a high-resolution microcomputed tomography (μ-CT). The μ-CT (SkyScan 1172; SkyScan; Kontich, Belgium) was set at a resolution of 11.56 μm, a voltage of 100 kV, a current of 100 μA, and an aluminum (Al + Cu) filter of 0.5 mm. The total rotation angle of the sample was 360° with a rotation step-size angle of 0.4°. Data were reconstructed using standardized cone–beam reconstruction software (NRecon v.1.6.9, SkyScan). The 3-D modeling and analysis involving porosity percentage, number and volume of pores, and degree of anisotropy were performed using CTAn v.1.13 (SkyScan Kontich, Belgium). The 3-D images were performed with the software CTvol v.2.2.3 (SkyScan Kontich, Belgium).

X-ray diffraction (XRD) was used to analyze the crystallography of the alloys and the L-1 powders. The experiment was performed using X-ray diffraction (D8-Discover/GADDS, Bruker, Karlsruhe, Germany) with a cobalt source radiation set at 40 kV and 40 mA, a 10–60° scanning angle, 0.02° step size, 1 s scan step time, and an integration time of 120 s. The EVA v.14 software (Bruker AXS, Karlsruhe, Germany) was used for phase identification and crystal size calculations following Scherrer's formula.

Fractured surface of CC, L-1, and L2- specimens were observed with scanning electron microscopy (SEM) (FE-SEM, FEI, Hillsboro, OR). SEM micrographs of the samples fractured by three-point bending were taken at 2500× magnification. The SEM was operated at 5–10 kV accelerating voltage, a spot size of 2–3 μm, and a working distance of 9.2–10.1 mm. To perform SEM backscattered electron imaging, the polished samples were etched for 30 s to reveal both the macrostructure and microstructure of the welds. The chemical etch was composed of a solution of 80% of hydrochloric acid (HCL) and 20% hydrogen peroxide (H_2O_2) (v/v) (Sigma Aldrich, St Louis, MO).[35] The SEM backscattering images were obtained with a SEM operated at 20 kV, spot size of 3 μm, and a working distance of 9.5–9.3 mm. The micrographs were taken at 200× magnification.

Biocompatibility assays

The releases of toxic metal ions from CC and L-1 alloys were measured using inductively coupled plasma atomic

TABLE II. Results (Mean ± SD) of Mechanical Tests for the Cast (CC) and Laser-Sintered (L-1 and L-2) Cobalt–Chrome Alloys

		CC	L-1	L-2
Technique precision error	(%)	9.5 (±6.5)	1.2 (±1.2)[a]	2.9 (±2.5)[a]
Elastic modulus	(GPa)	229 (±7)	202 (±16)[a,b]	225 (±10)
Bending yield strength	(MPa)	1462 (±142)	1626 (±118)[a]	1686 (±109)[a]
Flexural strength	(MPa)	2647 (±208)	2837 (±97)[a,b]	2602 (±106)
Fracture toughness	K_{1C} (MPa × $m^{1/2}$)	57.1 (±4.5)	61.2 (±2.1)[a,b]	56.1 (±2.3)
Fatigue resistance	0.2 mm deflection (%)	25.4 (±7.7)	91.1 (±4.2)[a]	89.6 (±4.7)[a]
	0.1 mm deflection (%)	47.9 (±18.3)	94.9 (±5.0)[a]	90.4 (±1.0)[a]
Hardness	(HV)	390 (±11) ‡	453 (±9)[a,c]	483 (±24)[a,c]
Density	Bulk (g/mm^3)	8.2 (±0.1)	8.0 (±0.0)[a,b]	8.4 (±0.1)
	Real (g/mm^3)	8.5 (±0.0)	8.3 (±0.1)[a,b]	8.6 (±0.0)
Porosity	(%)	2.2 (±0.7)	4.1 (±1.0)[a]	3.8 (±1.2)[a]

[a] Indicates a significant difference to cast (CC) group ($p < 0.05$).
[b] Indicates a significant difference between L-1 and L-2 groups ($p < 0.05$).
[c] Indicates a significant difference to hardness of teeth enamel ($p < 0.05$).

emission spectroscopy (ICP-AES; Perkin-Elmer, Wellesley, Mass). Each sample ($n = 6$) was immersed in 5 mL of PBS (phosphate buffered saline) simulating artificial saliva, and incubated for 7 days at 37°C.[25] The extracted solution was digested with 2 mL of concentrated nitric acid and then diluted in 7 mL of deionized water. Standard solutions containing Co, Cr, and Mo elements were prepared for calibration at a concentration of 2.0, 1.0, and 0.5 ppm (parts per million). Triplicate absorbance readings for all the above elements were recorded from each sample to determine the concentration of the elements released from the alloys in parts per million and these measurements were converted to units of micrograms per cm^2.

The cell biological response was studied *in vitro* using equally sized CC and L-1 specimens ($n = 9$) according to the international standard ISO 10993–5. Human gingival epithelial cells (HGEs) (Cedarlane Laboratories, Ontario, Canada) were cultured for 1, 3, and 7 days in serum free CnT-Prime medium (Cedarlane Laboratories, Ontario, Canada) in a 20% O_2 and 5% CO_2 humidified atmosphere at 37°C. HGEs were seeded at a density of 3×10^4 cells/cm^2 on the bottom of 24-well plates (Transwell, Costar, Corning, NY) while the Co–Cr metals were hanged on the middle of the well plates.

Two independent test kits for cell viability (Alamar Blue, Life technologies, Ontario, Canada) and cytotoxicity (CytotoxOne, PROMEGA, Wisconsin, USA) were combined to analyze the two different parameters from one single sample. After 24 h of cell culture, triplicates of 100 μL of the supernatant was transferred into a Microfluor 96-well fluorescence plate with clear bottom (Thermo Fisher Scientific, Waltham, MA) and mixed with 100 μL of cytotoxicity reagent. After an incubation of 10 min, the lactate dehydrogenase (LDH) release from damaged cells was analyzed by Spectra Max M2E (Molecular Device, Sunnyvale, CA). Then, 400 μL of cell culture media containing 10% of Alamar blue was added to each well and incubated for 4 h. The supernatant was then transferred into a 96-well plate with a clear bottom to detect the cell metabolism using a microplate reader (Spectramax M2E, Molecular Devices, CA, USA). For viability and cytotoxicity, the excitation and emission were 560 and 590 nm, respectively. Cells seeded without any metal exposure were considered as positive control. Metals without cells were incubated in parallel to serve as controls to remove the background fluorescence. Cell lysed with lysis solution provided with the cytotoxicity kit (2 μL/100 μL) were used to determine the maximum LDH release. The viability and cytotoxicity assays were repeated as described above; at 3 and 7 days in triplicates.

The live/dead staining assay for assessing the cytocompatibility of the metals was performed only at 24 h after seeding. The assay consisted of fluorescein diacetate (FDA) (Sigma, Steinheim, Germany, 5 mg in 1 mL of acetone) and propidium iodide (PI) (Sigma, Steinheim, Germany, 2 mg in 1 mL PBS). After removing the culture media from the well plates, a freshly prepared staining solution was added to each well and incubated for 5 min. Cells were analyzed and captured under the Zeiss AX10 fluorescence microscope (Carl Zeiss, Göttingen, Germany). Green fluorescence indicates viable cells and red fluorescence dead cells.

Statistical analysis

Statistical analysis for the mechanical and biocompatibility data was performed with the software Origin 8.0 (Origin lab, Northampton, MA). Mean and standard deviation (SD) values were calculated for all measurements. A one-way analysis of variance (ANOVA) and Tukey HSD multiple comparison test were used to test for statistical differences of mechanical and physical properties between the CC, L-1, and L-2 groups. The statistical differences for the biocompatibility test between CC and L-1 groups were tested using Student's *t* test. The significance level was set at $p < 0.05$.

RESULTS

Table II provides an overview of all the results obtained from the mechanical and physical characterization techniques. The precision error that was calculated based on the dimensional comparison between the CAD designed specimen and the fabricated one indicated that both laser-sintering techniques (L-1 and L-2) were up to 8 times more precise than the conventional casting technique (CC) ($p < 0.05$) (Figure 1). The precision error of CC samples was 9.3 ± 6.5%, while the precision errors of L-1 and L-2 were

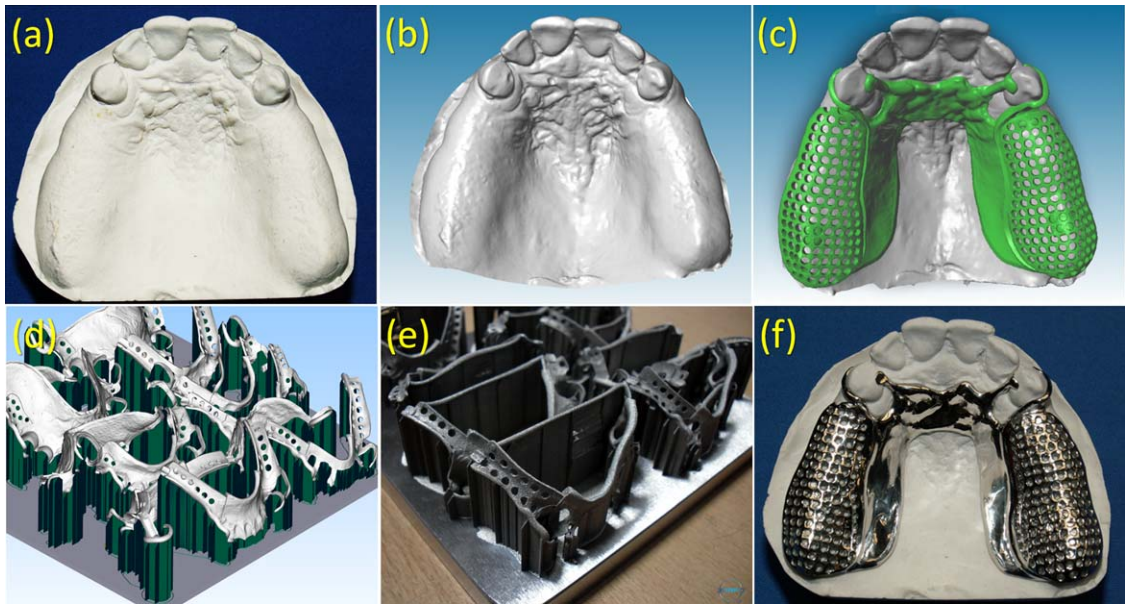

FIGURE 1. Photographs illustrating the process of designing and fabricating removable partial dentures (RPDs) framework using laser-sintering technique: (a) master cast of partially edentulous arch, (b) 3-D scan of the model, (c) designing of RPDs framework, (d) placing RPDs frameworks in a digital platform, (e) processed RPDs frameworks in the producing platform, and (f) the final RPD framework.

$1.2 \pm 1.2\%$ and $2.9 \pm 2.5\%$, respectively. The results of the three-point bending test indicated that the elastic modulus of the L-1 alloys were significantly lower (202 ± 16 GPa) than the CC alloys (229 ± 7 GPa) and the L-2 alloys (225 ± 10 GPa). The bending yield strength of the L-1 and L-2 alloys were significantly higher (1626 ± 118 and 1685 ± 109 MPa, respectively) than the CC alloys (1462 ± 142 MPa). The flexural strength and fracture toughness of the L-1 alloys (2837 ± 97 MPa and 61.2 ± 2.1 1 MPa $\times$ $m^{1/2}$) were significantly higher than the CC (2647 $\pm$208 MPa and 57.1 ± 4.5 MPa $\times$ $m^{1/2}$) and L-2 alloys (2602 ± 106 MPa and 56.1 ± 2.3 1 MPa $\times$ $m^{1/2}$).

Both L-1 and L-2 samples presented higher ($p < 0.05$) resistance to fatigue than the CC samples after 6000 stress cycles simulating the insertion and removal of the dentures from the mouth for 5 years (Figure 2 and Table III). The fatigue resistance tests of the L-1 and L-2 groups showed that they maintained 91.1% and 89.6% of their original stress, respectively, at 0.2 mm deflection. Whereas, the CC group maintained only 25.4% of the original stress (Figure 2 and Table II). Similar fatigue resistance behavior was recorded at 0.1 mm deflection for all groups.

The microhardness values of the L-1 and L-2 alloys (453 ± 9 and 477 ± 14 HV, respectively) were higher ($p < 0.05$) than CC alloys (390 ± 11 HV), and the L-2 group had higher microhardness than L-1 group ($p < 0.05$) (Table II). However, all alloys had higher microhardness than tooth enamel (353 ± 40 HV). CC and L-2 alloys had similar bulk density and real density; however, the density of the L-1 alloys was lower than CC and L-2 alloys ($p < 0.05$). In addition, the L-1 alloys had a higher total porosity than the CC alloys ($p < 0.05$), but not the L-2 alloys (Table II). The porosity of L-1 and L-2 alloys was mainly closed porosity, and more isotropic ($p < 0.05$) than in the CC alloys (Table III and Figure 3).

The XRD crystallographic analysis (Figure 4) of the structure of CC, L-1, L-2 alloys, and L-1 powders revealed that the face-centered cubic (fcc) phase, which is characteristic of Co–Cr, was present in all groups as evident in Figure 4. However, the L-1 alloys showed an additional hexagonal close-packed (hcp) phase of Co–Mo that was not present in the other groups. The XRD spectra showed that the crystal size of CC (16.3 ± 2.2 nm) and L-2 (16.2 ± 2.1 nm) alloys was similar, but larger than the crystal size of both the L-1 alloys (14.6 ± 1.1 nm) and the L-1 powder (14.3 ± 1.8 nm) ($p < 0.05$).

The digital photographs and SEM back-scattered electron images of the polished surfaces of CC, L-1, and L-2 alloys are shown in Figure 4. The polished surfaces of the CC alloys revealed large grains while the polished surfaces of the L-1 and L-2 alloys exhibited a fine microstructural appearance. SEM observations of fractured samples from the different alloys are demonstrated in Figure 5. These SEM images revealed that the L-1 and L-2 alloys present an organized stop-like fracture path, whereas the CC alloys demonstrate an unorganized fracture path.

Biocompatibility assays showed that both L-1 and CC alloys had comparable behaviors (Figure 6 and Table IV). Overall, the trace amounts of elements released from CC and L-1 alloys were within a small range. Both L-1 and CC alloys released comparable amounts of Co, Cr, and Mo, but only the release of Co was significantly higher in the L-1 alloys when compared to the CC alloys. The percentage of cell activity (relative to control cells unexposed to metal) of

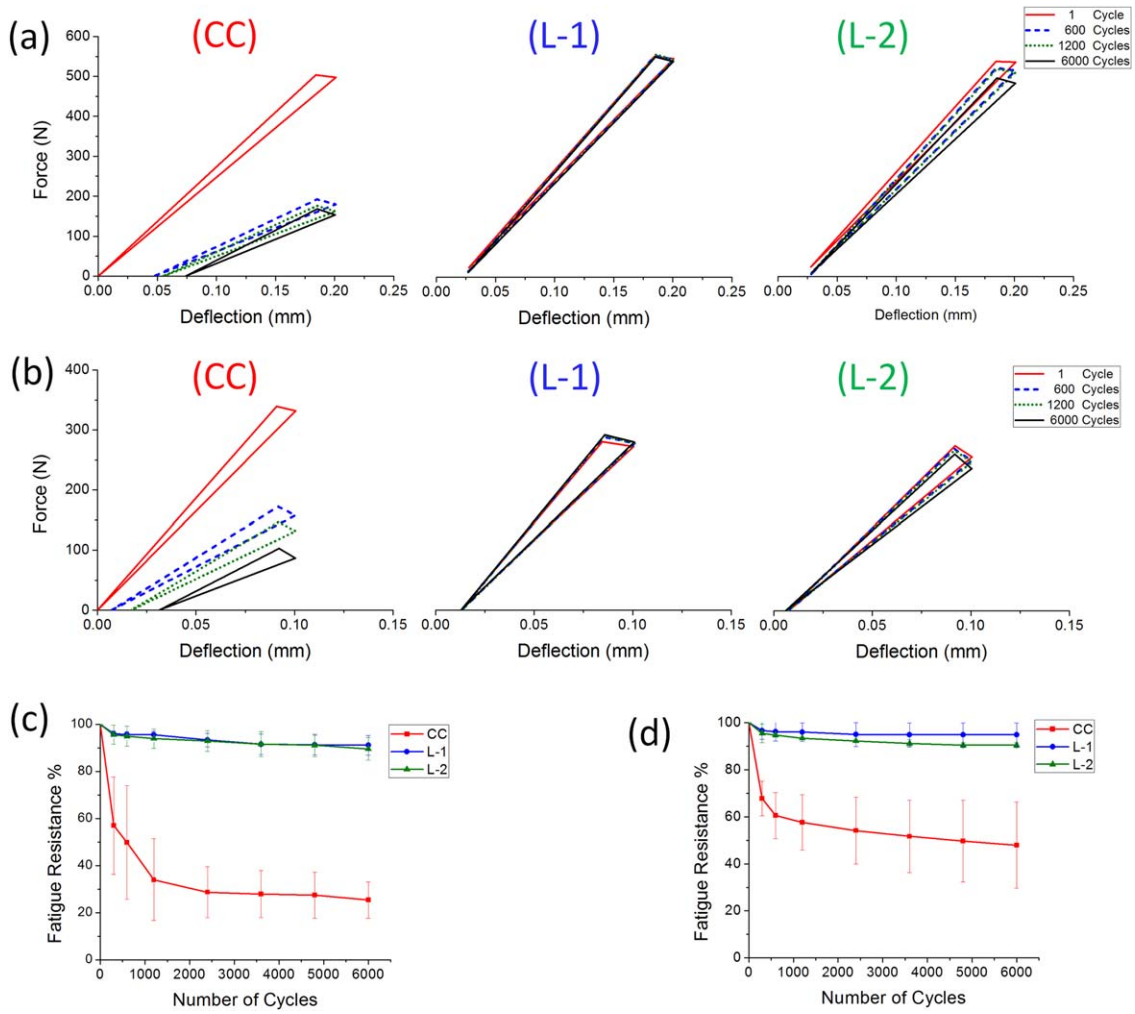

FIGURE 2. Load/deflection diagrams showing cycles of loading and unloading of the cast (CC) and laser-sintered (L-1 and L-2) Co–Cr alloys for a deflection of (a) 0.2 mm and (b) 0.1 mm. Percentage of the fatigue resistance comparing the postfatigue force with the initial force at a deflection (c) 0.2 mm and (d) 0.1 mm.

the two groups are illustrated in Figure 6. The viability and cytotoxicity of cells exposed to the L-1 and CC alloys declined over time up to 7 days in comparison to cells not exposed to Co–Cr alloys. However, no statistical difference was found between L-1 and CC alloys in terms of the viability and cytotoxicity. Figure 6(c–f) shows the results of the live/dead assays of cells cultured for 24 h and exposed to L-1 and CC alloys.

DISCUSSION

This study was designed to characterize the mechanical, physical, and biocompatibility properties of laser-sintered RPD Co–Cr alloy and compare them to those of the cast RPD Co–Cr alloys. In this study, the Co–Cr alloys were fabricated using two commercially available systems, Phenix and EOS, which are based on two different laser-sintering methods, SLS and DMLS, respectively. The materials and

TABLE III. μ-CT Scan Analysis Results for the Cast (CC) and Laser-Sintered (L-1and L-2) Co–Cr Alloys. Values Presented as Mean ± SD

		CC	L-1	L-2
Number of pores		4610 (±693)	5507 (±573)[a]	5522 (±644)[a]
Closed porosity percentage	(%)	1.63 (±0.56)	2.63 (±0.72)[a]	1.96 (±0.44)[a]
Open porosity percentage	(%)	0.50 (±0.44)	0.69 (±0.39)	0.64 (±0.46)
Total volume of pores	(mm^3)	0.02 (±0.01)	0.03 (±0.01)[a,b]	0.02 (±0.01)
Total porosity percentage	(%)	2.13 (±0.85)	3.32 (±1.06)[a]	2.60 (±0.80)
Degree of porosity anisotropy		0.71 (±0.04)	0.67 (±0.03)[a,b]	0.47 (±0.11)[a]

[a] Indicates a significant difference to cast (CC) group ($p < 0.05$).
[b] Indicates a significant difference between L-1 and L-2 groups ($p < 0.05$).

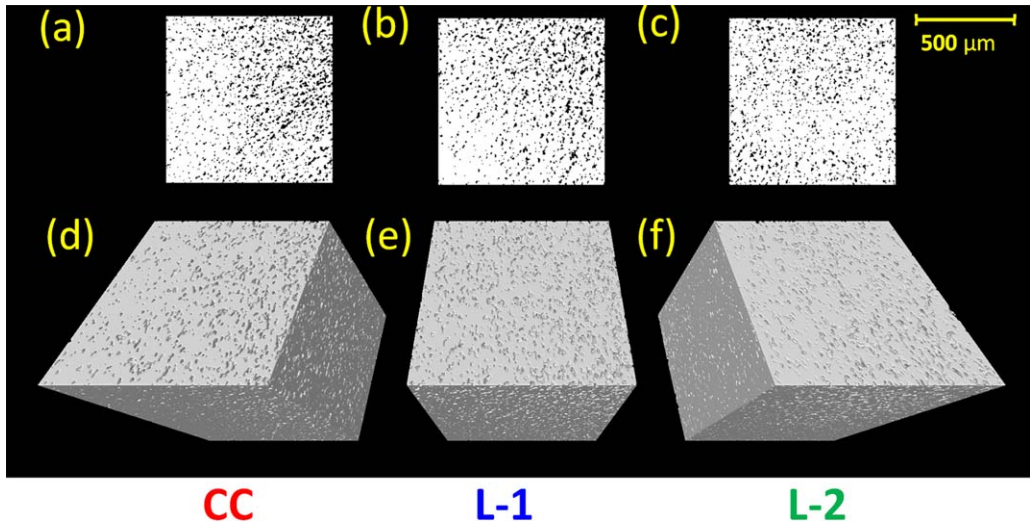

FIGURE 3. (a–c) Two-dimensional images and (d–f) 3-D images by μ-CT showing the porosity of the cast (CC) and laser-sintered (L-1 and L-2) Co–Cr alloys.

processing parameters were specified for each system according to the respective manufacturer's instructions, and they were not exactly the same (Table I). This might render the comparison difficult. However, the differences in chemical composition between the CC group and L-1 group were very small, and this would suggest that the characterization differences observed between the groups were most probably due to the processing approach of each system.

To the best of our knowledge, this is the first study assessing the fatigue resistance of laser-sintered Co–Cr alloys, as compared to that of the cast Co–Cr alloy. Fabricating RPDs by laser-sintering technology can have an economic impact on the way RPDs are made as well as improve the quality of RPDs. This will have a high impact on the millions of patients around the world who wearing RPDs. In fact, it was found in this study that the laser-sintering technique was 6–8 times more precise and 3 times more accurate than the casting technique. It was suggested that the high precision of laser-sintering technique was due to reduced number of accumulated of errors that occur at the different steps during casting process. Although there was no a significant difference between the precision error of L-1 and L-2 techniques, the L-1 samples, which were processed by the Phenix system, tend to be more accurate than the L-2 group processed by the EOS system. The reason for these accuracy discrepancies between L-1 and L-2 could most probably be related to the features of the system since only L-1 (Phenix system) use a roller to compact the powder.

Mechanical properties

Clasp failure, which is the retentive elements engaging the teeth, is the most common complication of RPDs, and it is the main reason why most RPDs are replaced after 5–6 years of use.[22,23] These failures are caused by the excessive and repeated stress on clasps during insertion and removal of the dentures from the mouth.[22,23] This repeated stress might also result in fatigue failure and deformation of the RPD clasps, which eventually lead to the loss of retention.[23] For this reason, in our study, the three-point bending and fatigue tests were performed to simulate the long-term function of the RPDs in the patients' mouth during insertion and removal of the dentures from the mouth.

The results obtained from the three-point bending test (Table II) demonstrated that the L-1 alloys have a lower elastic modulus than the CC and L-2 alloys. This analysis indicates that L-1 alloys are more flexible and less stiff than CC and L-2 alloys. The elastic modulus of L-1 is closer to that of teeth (80–94 GPa)[36] than CC and L-2. This lower stiffness can be an advantage because it could minimize damage inflicted to the underlying teeth when fabricating RPDs made of L-1 alloys.[37] The reason for that is when the stiffness of an RPD framework surpasses that of supporting tissues (e.g., teeth), high-stress concentration accumulates at the metal–tissue interface resulting in fracture of the weaker component, which is the tooth in this case.[38] However, stiff Co–Cr alloys are favorable for RPDs components that require high stiffness, such as rests and connectors, to prevent distortion and deflection of the dentures.[22] Therefore, L-1 alloys would be more favorable for fabricating the RPDs' clasps, but less favorable than L-2 and CC alloys for fabricating the other RPDs components, such as rests and connectors.

The bending yield strength of both L-1 and L-2 alloys were higher than CC alloys. The bending yield strength is considered the most important mechanical property for RPDs since higher values of this strength helps to resist the plastic (permanent) deformation of RPD's clasps, and thus preventing their failure.[39] In addition, the flexural strength and fracture toughness of the L-1 group were higher than the CC and L-2 groups. Processing Co–Cr alloy by the DMLS method (L-2) involves full melting of some metal powder which makes it closer to the casting method than SLS method. This might be the reason of mechanical properties

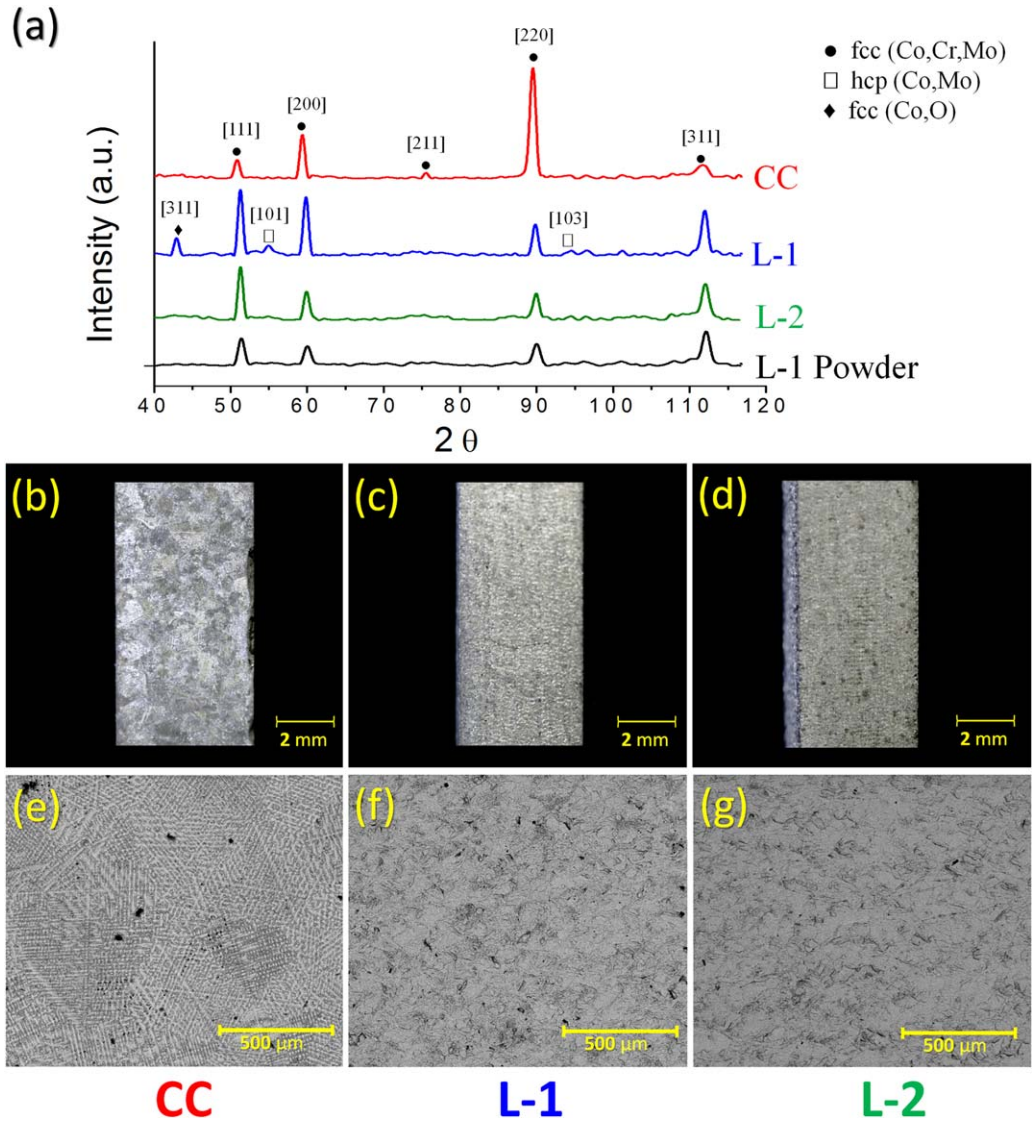

FIGURE 4. (a) Representative XRD spectra of the cast (CC), laser-sintered (L-1 and L-2) Co–Cr alloys and the metal powder used for laser-sintering, (b–d) digital photograph images, and (e–g) SEM Back-scattering images on polished surfaces of the CC, L-1, and L-2 alloys.

similarity between L-2 and CC alloys. Generally, L-1 alloys have better mechanical properties for RPDs than other alloys in term of the elasticity and strength, and this might be related to their porosity and microstructure which will be discussed later.[40]

The fatigue resistance test was performed to simulate the insertion and removal of the dentures from the mouth for the period of 5 years (Figure 2 and Table II).[41] Clasps of the RPDs usually engage undercuts on the abutment tooth surface that are 0.25 mm deep.[2] To release a clasp from the abutment tooth, the clasp arm is bent to reach a deflection that equals to the depth of the undercut. This was simulated in the performed fatigue resistance test by bending the alloys to deflections of 0.1 and 0.2 mm. The results of the fatigue resistance test showed that alloys processed by laser-sintering technique (L-1 and L-2) had higher resistance to fatigue than those fabricated by the casting technique. In addition, the L-1 and L-2 alloys maintained most of their original mechanical properties after the fatigue cycles, whereas the CC alloys underwent a dramatic deformation, which was even more pronounced after fatigue cycles of larger deflections (Figure 2). Based on our *in vitro* study, the average survival rate of the laser-sintered RPDs would be much higher than that of the cast RPDs, which is reported to have an average survival rate of 5.5 years.[23]

The high-fatigue resistance of L-1 and L-2 alloys is attributed to their high bending yield strength that allows higher resistance to plastic deformation when compared to CC alloys (Table II).[39] As suggested by Koutsoukis et al., the high bending yield strength and fatigue resistance of laser-sintered alloys could be attributed to their crystallinity and homogeneous microstructure (Figures 4 and 5).[6] The SEM observation (Figure 5) of the CC, L-1, and L-2 alloys at the fractured surfaces showed that the L-1 and L-2 alloys were more homogenous than the CC alloys. The fine microstructure of the L-1 and L-2 alloys was due to rapid solidification

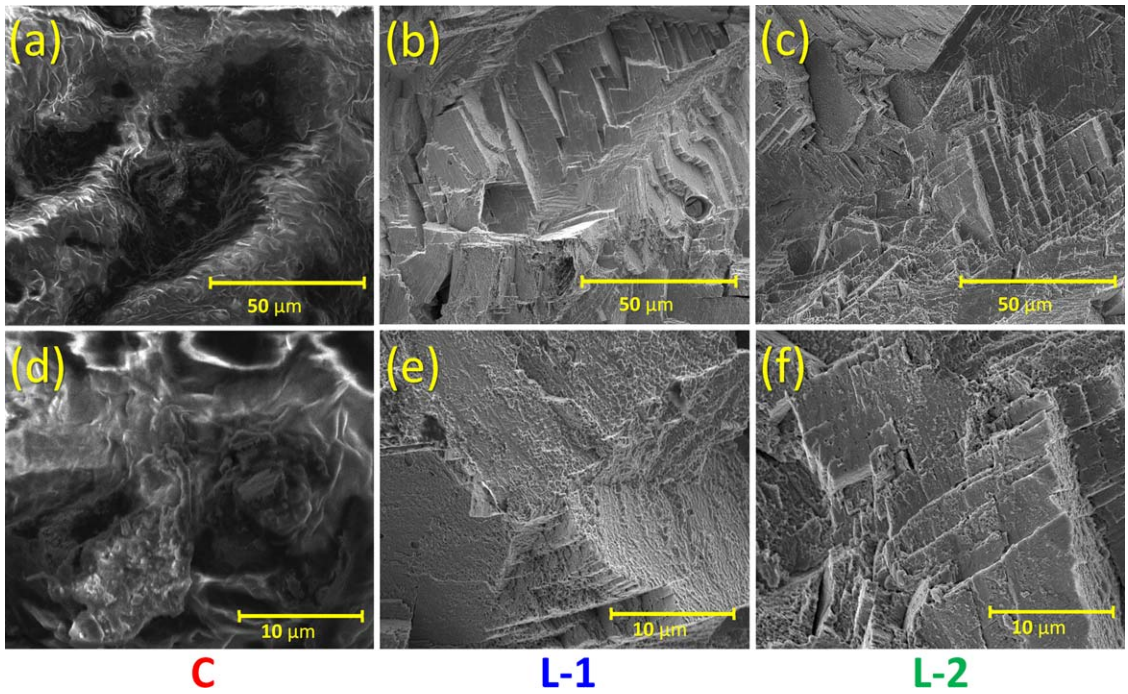

FIGURE 5. Representative SEM micrograph at the fractured surfaces of the cast (CC) and laser-sintered (L-1 and L-2) Co–Cr alloys at magnifications of 2500× and 10,000×.

of the melted powder, while the irregular microstructure of the CC alloy could be probably due to the internal defects and impurities that occur during the casting technique.[6,25] As a result of the homogenous microstructure of the L-1 and L-2 alloys, wedge-type cracks and organized fracture paths were observed in L-1 and L-2 alloys, while unorganized fracture paths were observed in the CC alloys (Figure 5). Having a homogenous microstructure is beneficial for reducing the failures of RPDs clasps because it promotes homogeneous slip deformation, which in turn reduces the residual

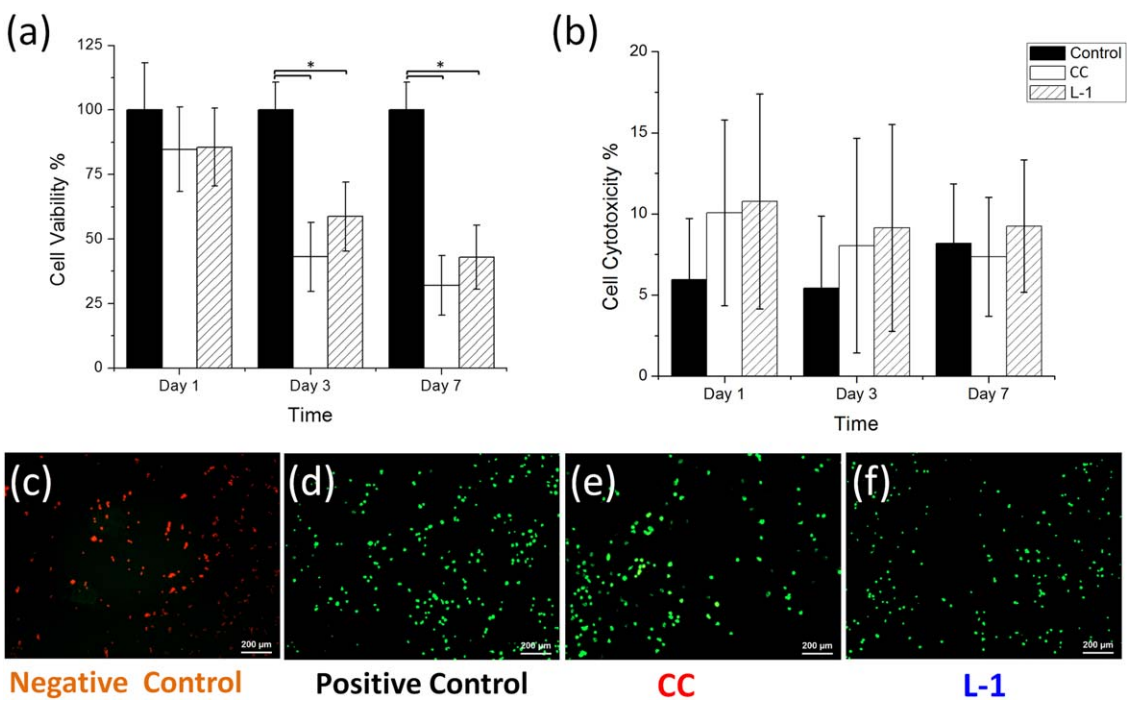

FIGURE 6. Percentage of (a) mean cell viability and (b) cell cytotoxicity (relative to control) of the cast (CC) and laser-sintered (L-1) Co–Cr alloys. Error bars represent SD and * indicates a significant difference between the different groups ($p < 0.05$). (c–f) Live/dead staining results after 24 h of incubation for CC and L-1 alloys showing a higher number of live cells present (green) in compare to dead cells (red) in the negative control.

TABLE IV. Element Release in μg/cm² (Mean ± SD) From Cast (CC) and Laser-Sintered (L-1) Co–Cr Alloys

	Cobalt (Co)	Chromium (Cr)	Molybdenum (Mo)
CC	0.699 (±0.392)	0.007 (±0.027)	0.065 (±0.079)
L-1	1.196 (±0.044)*	0.005 (±0.025)	0.136 (±0.021)

[a]Indicates a significant difference to cast (CC) group ($p < 0.05$).

stresses and stress concentrations, as opposed to the nonhomogeneous microstructure observed in the CC samples.[6]

Both types of laser-sintered alloys (L-1 and L-2) were significantly harder than the cast (CC) alloy (Table II). High hardness values are desirable in the RPDs for resisting the scratching of the metallic alloy.[42] However, all the alloys tested in this study were harder than tooth enamel, and this might damage the teeth during insertion and removal the RPDs from the mouth. It should be noted that tooth damage can still occur due to the friction between the harder metal and the softer tooth tissue even in the presence of saliva in the oral cavity that acts as a lubricant. One way to tackle this potential problem is to use metallic alloys with an appropriate elastic of modulus, as the friction depends on the force exerted by the clasp on the tooth. Accordingly, the lower elastic modulus of the L-1 alloy could palliate the negative consequence of its high hardness of Co–Cr alloys.

Physical properties

The porosity percentage of all the alloys tested in this study was minimal. Usually, the cast metals present high porosities and internal defects due to gas inclusion during the fabrication process.[6,22] However, the minimal porosity of the CC alloys observed in this study could be attributed to the flat geometry of the samples and their relative small size, which might have reduced the gas inclusion. In addition, the porosity percentages for both laser-sintered alloys were minimal because of the postheat treatment that was applied to the alloys after processing.[12,43] It is known that the porosity of the laser-sintered alloys can be influenced and controlled by the operating parameters of the laser-sintering technology, such as layer thickness, laser power, laser wavelength, and scanning speed.[6,10] In this study, the total porosity percentage was 1–2% higher in the L-1 alloys than in the CC and L-2 alloys (Tables II and III). This could be attributed to the fusion of the metal powder during the laser-sintering process that might increase the number of internal porosities between the sintered particles and between the different layers.[6,10,11] Furthermore, this could explain why the L-1 alloys presented lower density than alloys fabricated using the L-2 and CC techniques.

Although the porosity of L-1 alloys was slightly higher than that of CC alloys, the majority of pores in L-1 alloys were closed. Whereas, the percentage of open porosity was similar in all alloys (Table III and Figure 3). It is known that open porosities can become surface sites for crack initiation, and therefore, influence the fatigue resistance of the alloys.[7,22,25] Therefore, the fact that closed porosity influences the fatigue resistance less than open porosity might be the reason of the relatively low elastic modulus of L-1 alloys in this study.[40] On the other hand, our results showed that the porosity in the L-1 and L-2 alloys was more isotropic than in the CC group (Figure 3 and Table III). This indicates that the porosities in L-1 and L-2 alloys are more oriented within the same volume than in the CC samples. Therefore, the homogeneity of both porosity and microstructure of L-1 and L-2 alloys could be another factor that explains the higher fatigue resistance of the laser-sintered alloys over the cast ones, despite having similar open porosities.

XRD analysis showed that both L-2 and CC alloys yielded similar crystallographic patterns [Figure 4(a)]; however, the XRD pattern L-1 alloys exhibited peaks referring to a hexagonal close-packed (hcp) phase of Co-Mo, which is in agreement with a previous study.[24] This could be a result of the phase transformation from (fcc) to (hcp) phase during the rapid cooling of the laser-sintering process since the (fcc) phase forms at high transformation temperatures as opposed to the (hcp) phase that forms at lower temperatures.[6,42] Indeed, unlike the DMLS method (EOS system), the metal powder of L-1 alloys processed by SLS method (Phenix system) is exposed to temperatures below its phases transition.[12] Previous studies reported that the observed (hcp) phase influences the mechanical properties of the alloys and improves their strength, wear resistance, and hardness, which further confirms our results.[6,44]

XRD analysis also revealed that the Co–Cr powder and L-1 alloys had similar crystal size, while the crystal size of the CC and L-2 alloys was larger than that of the L-1 alloys, which is most probably due to the solidification of the melted metal.[20] Optical photograph and SEM back-scattering images of the polished etched surfaces of L-1 and L-2 alloys demonstrated a fine microstructure, whereas the CC alloys showed different grain boundaries within the surface [Figure 4(b–g)]. The smaller size of crystal and grain and the homogeneity in the microstructure that of the L-1 and L-2 alloys have a positive impact on the mechanical and fatigue properties of the alloys.[6,45] In summary, this study suggests that both L-1 and L-2 alloys are more suitable to be used in the fabrication of the RPD than the CC alloys because of their fatigue and physical properties.

Biocompatibility

Biocompatibility assays revealed that both L-1 and CC alloys had similar behaviors (Figure 6 and Table IV). Both alloys released cobalt (Co), chromium (Cr), and molybdenum (Mo) to the simulated saliva media (PBS). Compared to the other elements, the release of Co was found to be relatively much higher from both alloys, and this is probably because Co is the major element (64%) in the composition of the Co–Cr alloys. Even though the L-1 alloys released higher amount of Co than the CC alloys, the amount of Co released from both alloys was safe and far below the recommended daily dietary intake (i.e., Co $\leq$ 50 μg/day).[26]

The viability of human gingival epithelial cells was comparable in all groups on day 1; however, the proliferation rate of cells exposed to the L-1 and CC alloys declined over time in comparison to cells not exposed to the Co-Cr alloys

(Figure 6). This can be attributed to the fact that the released Co inhibits cell growth.[46,47] However, the cytotoxicity assays revealed that cells exposed to the L-1 and CC Co–Cr alloys behaved similarly to cells not exposed to Co–Cr alloys. Therefore, these results suggest that laser-sintered Co–Cr alloys are biocompatible and present similar biocompatibility properties when compared to the traditional cast Co–Cr alloys that are currently commonly used in the oral cavity.

CONCLUSION

Co–Cr alloys processed by the laser-sintering techniques are more precise and present better fatigue resistance and mechanical properties for RPDs than cast alloys due to their better homogeneity and small grain size. Moreover, both laser-sintered and cast Co–Cr alloys present similar biocompatibility properties. Accordingly, laser-sintered RPDs could present clinical benefits over cast ones in terms of fitting and mechanical stability.

ACKNOWLEDGMENT

The authors thank Dr Ahmed Al Subaie and Ms Linda Harrison for their technical support.

REFERENCES

1. Preshaw P, Walls A, Jakubovics N, Moynihan P, Jepson N, Loewy Z. Association of removable partial denture use with oral and systemic health. J Dent 2011;39:711–719.
2. Carr AB, Brown DT. McCracken's Removable Partial Prosthodontics. Saint Louis, MO: Elsevier Mosby; 2011.
3. Hummel SK, Wilson MA, Marker VA, Nunn ME. Quality of removable partial dentures worn by the adult U.S. population. J Prosthet Dent 2002;88:37–43.
4. Sun S-H, Koizumi Y, Kurosu S, Li Y-P, Matsumoto H, Chiba A. Build direction dependence of microstructure and high-temperature tensile property of Co–Cr–Mo alloy fabricated by electron beam melting. Acta Biomater 2014;64:154–168.
5. Venkatesh KV, Nandini VV. Direct metal laser sintering: A digitised metal casting technology. J Indian Prosthodont Soc 2013;13: 389–392.
6. Koutsoukis T, Zinelis S, Eliades G, Al-Wazzan K, Rifaiy MA, Al Jabbari YS. Selective laser melting technique of Co–Cr dental alloys: A review of structure and properties and comparative analysis with other available techniques. J Prosthodont 2015.
7. Vallittu PK, Miettinen T. Duration of induction melting of cobalt-chromium alloy and its effect on resistance to deflection fatigue of cast denture clasps. J Prosthet Dent 1996;75:332–336.
8. Puskar T, Jevremovic D, Williams RJ, Eggbeer D, Vukelic D, Budak I. A Comparative analysis of the corrosive effect of artificial saliva of variable pH on DMLS and cast Co–Cr–Mo dental alloy. Materials 2014;7:6486–6501
9. Lima JMC, Anami LC, Araujo RM, Pavanelli CA. Removable partial dentures: Use of rapid prototyping. J Prosthodont 2014;23:588–591.
10. Van Noort R. The future of dental devices is digital. Dent Mater 2012;28:3–12.
11. Akova T, Ucar Y, Tukay A, Balkaya MC, Brantley WA. Comparison of the bond strength of laser-sintered and cast base metal dental alloys to porcelain. Dent Mater 2008;24:1400–1404.
12. Kruth J-P, Mercelis P, Van Vaerenbergh J, Froyen L, Rombouts M. Binding mechanisms in selective laser sintering and selective laser melting. Rapid prototyping J 2005;11(1): 26–36.
13. Ahn D.-G. Direct metal additive manufacturing processes and their sustainable applications for green technology: A review. Int J Precis Eng Man 2016;3(4): 381–395.
14. Mazzoli A. Selective laser sintering in biomedical engineering. Med Biol Eng Comput 2013;51(3): 245–256.
15. Vayre B, Vignat F, Villeneuve F. Metallic additive manufacturing: State-of-the-art review and prospects. Mech Ind 2012;13(2): 89–96.
16. Ahn D.-G. Applications of laser assisted metal rapid tooling process to manufacture of molding & forming tools—state of the art. Int J Precis Eng Man 2011. 12(5): 925.
17. Cheah CM, Chua CK, Lee CW, Feng C, Totong K. Rapid prototyping and tooling techniques: A review of applications for rapid investment casting. Int J Adv Manuf Tech 2005; 25(3): 308–320.
18. Khaing MW, Fuh JYH, Lu L. Direct metal laser sintering for rapid tooling: Processing and characterisation of EOS parts. J Mater Process Technol 2001;113(1–3): 269–272.
19. Hollander DA, von Walter M, Wirtz T, Sellei R, Schmidt-Rohlfing B, Paar O, Eril HJ. Structural, mechanical and in vitro characterization of individually structured Ti–6Al–4V produced by direct laser forming. Biomaterials 2006;27:955–963.
20. Vandenbroucke B, Kruth J-P. Selective laser melting of biocompatible metals for rapid manufacturing of medical parts. Rapid Prototyping J 2007;13:196–203.
21. Zhang B, Huang Q, Gao Y, Luo P, Zhao C. Preliminary study on some properties of Co-Cr dental alloy formed by selective laser melting technique. J Wuhan Univ Technol 2012;27:665–668.
22. Gapido CG, Kobayashi H, Miyakawa O, Kohno S. Fatigue resistance of cast occlusal rests using Co-Cr and Ag-Pd-Cu-Au alloys. J Prosthet Dent 2003;90:261–269.
23. Sandu L, Faur N, Bortun C. Finite element stress analysis and fatigue behavior of cast circumferential clasps. J Prosthet Dent 2007;97:39–44.
24. Al Jabbari YS, Koutsoukis T, Barmpagadaki X, Zinelis S. Metallurgical and interfacial characterization of PFM Co–Cr dental alloys fabricated via casting, milling or selective laser melting. Dent Mater 2014;30:e79–e88.
25. Xin XZ, Xiang N, Chen J, Wei B. In vitro biocompatibility of Co–Cr alloy fabricated by selective laser melting or traditional casting techniques. Mater Lett 2012;88:101–103.
26. Wataha JC. Biocompatibility of dental casting alloys: A review. J Prosthet Dent 2000;83:223–234.
27. Hedberg YS, Qian B, Shen Z, Virtanen S, Wallinder IO. In vitro biocompatibility of CoCrMo dental alloys fabricated by selective laser melting. Dent Mater 2014;30(5): 525–534.
28. Bae EJ, Jeong ID, Kim WC, Kim JH. A comparative study of additive and subtractive manufacturing for dental restorations. J Prosthet Dent 2017.
29. Alageel O, Abdallah M-N, Luo ZY, Del-Rio-Highsmith J, Cerruti M, Tamimi F. Bonding metals to poly(methyl methacrylate) using aryldiazonium salts. Dent Mater 2015;31:105–114.
30. Callister WD. Fundamentals of Materials Science and Engineering: An Integrated Approach. Hoboken, NJ: John Wiley & Sons; 2005.
31. Chermant J, Osterstock F. Fracture toughness and fracture of WC-Co composites. J Mater Sci 1976;11:1939–1951.
32. Brynk T, Laptiev A, Tolochyn O, Pakiela Z. The method of fracture toughness measurement of brittle materials by means of high speed camera and DIC. Comput Mater Sci 2012; 64: 221–224.
33. Ghadimi E, Eimar H, Song J, Marelli B, Ciobanu O, Abdallah M-N, Stähli C, Nazhat S, Vali H, Tamimi F. Regulated fracture in tooth enamel: A nanotechnological strategy from nature. J Biomech 2014;47:2444–2451.
34. Abdallah M-N, Eimar H, Bassett DC, Schnabel M, Ciobanu O, Nelea V, McKee MD, Cerruti M, Tamimi F. Diagenesis-inspired reaction of magnesium ions with surface enamel mineral modifies properties of human teeth. Acta Biomater 2016;37:174–183.
35. Viennot S, Dalard F, Lissac M, Grosgogeat B. Corrosion resistance of cobalt-chromium and palladium-silver alloys used in fixed prosthetic restorations. Eur J Oral Sci 2005;113:90–95.
36. Rees JS, Jacobsen PH. Elastic modulus of the periodontal ligament. Biomater 1997;18:995–999.
37. Combe EC, Shaglouf AMS, Watts DC, Wilson NHF. Mechanical properties of direct core build-up materials. Dent Mater 1999;15: 158–165.
38. Currey JD. How well are bones designed to resist fracture? J Bone Miner Res 2003;18:591–598.
39. Mahmoud A, Wakabayashi N, Takahashi H, Ohyama T. Deflection fatigue of Ti-6Al-7Nb, Co-Cr, and gold alloy cast clasps. J Prosthet Dent 2005;93:183–188.

40. Greiner C, Oppenheimer SM, Dunand DC. High strength, low stiffness, porous NiTi with superelastic properties. Acta Biomater 2005;1:705–716.
41. Lassila LVJ, Vallittu PK. Effect of water and artificial saliva on the low cycle fatigue resistance of cobalt-chromium dental alloy. J Prosthet Dent 1998;80:708–713.
42. Barucca G, Santecchia E, Majni G, Girardin E, Bassoli E, Denti L, Gatto A, Iuliano L, Moskalewicz T, Mengucci P. Structural characterization of biomedical Co–Cr–Mo components produced by direct metal laser sintering. Mater Sci Eng 2015;48:263–269.
43. AlMangour B, Grzesiak D, Yang J-M. Selective laser melting of TiB2/H13 steel nanocomposites: Influence of hot isostatic pressing post-treatment. J Mater Process Technol 2017;244: 344–353.
44. Moharrami N, Langton DJ, Sayginer O, Bull SJ. Why does titanium alloy wear cobalt chrome alloy despite lower bulk hardness: A nanoindentation study? Thin Solid Films 2013;549: 79–86
45. Wu L, Zhu H, Gai X, Wang Y. Evaluation of the mechanical properties and porcelain bond strength of cobalt-chromium dental alloy fabricated by selective laser melting. J Prosthet Dent 2014; 111:51–55.
46. Berstein A, Bemauer I, Marx R, Geurtsen W. Human cell culture studies with dental metallic materials. Biomaterials 1992; 13:98–100.
47. Bearden L, Cooke F. Growth inhibition of cultured fibroblasts by cobalt and nickel. J Biomed Mater Res 1980;14:289–309.